Journal of Computational Acoustics, Vol. 14, No. 1 (2006) 21–43

INTERNATIONAL ASSOCIATION
FOR MATHEMATICS AND
COMPUTERS IN SIMULATION

NUMERICAL ANALYSIS OF A COUPLED FINITE-INFINITE ELEMENT METHOD FOR EXTERIOR HELMHOLTZ PROBLEMS

JEAN-CHRISTOPHE AUTRIQUE
LMS International, Interleuvenlaan 70
Researchpark Haasrode Z1, 3001 Leuven, Belgium
jean-christophe.autrique@lms.be

FRÉDÉRIC MAGOULÈS*
Université Henri Poincaré, Institut Elie Cartan de Nancy
BP 239, 54506 Vandoeuvre-les-Nancy Cedex, France
frederic.magoules@iecn.u-nancy.fr

Received 1 May 2004
Revised 1 September 2004

Coupled finite-infinite element computations are very efficient for modeling large scale acoustics problems. Parallel algorithms, like sub-structuring and domain decomposition methods, have shown to be very efficient for solving huge linear systems arising from acoustics. In this paper, a coupled finite-infinite element method is described, formulated and analyzed for parallel computations purpose. New numerical results illustrate the efficiency of this method for academic test cases and industrial problems alike.

Keywords: Infinite element; finite element; parallel computing; acoustic scattering; SYSNOISE.

1. Introduction

The finite element solution of acoustic problems usually involves huge meshes since the mesh size should be proportional to the frequency of the problem in order to have a good approximation of the solution. So, the discretization leads to an extremely large linear system of equations with a sparse matrix. This becomes a crucial point for acoustic scattering problems where the domain around the scattered object is unbounded. If one wants to keep the sparsity of the matrix and reduce the number of unknowns of the linear system, the infinite element methods[1–3] are an efficient alternative to the boundary element methods which leads to a dense matrix,[4,5] or to the absorbing boundary conditions which should be defined far enough from the object.[6–9] The accuracy of the infinite element methods is linked with a parameter called the order of the infinite element. The highest this order, the smallest the error between the approximate solution and the exact solution. Unfortunately,

*Corresponding author.

increasing the value of this parameter tends to deteriorate the conditioning number of the assembly matrix.[10–12] Additionally the infinite element methods can only be applied for convex objects. A remedy of this drawback is to use a coupled finite-infinite element formulation. The coupled method consists of surrounding the object with a convex envelope. The volume between the object and the convex envelope is meshed with finite elements, and infinite elements are defined on the surface of the convex envelope.

The iterative methods used to solve the linear system of equations arising from the discretization are very easy to program.[13] Preconditioning techniques based on substructuring can additionally be applied.[14] The domain decomposition methods for example, are based on a mesh partitioning of the global domain. Then the methods consist of solving iteratively a linear system defined at the interface between the subdomains, and each iteration of the algorithm involves a direct solution of an acoustic problem inside each subdomain. Such methods are very well suited for distributed parallel computing. In the case of a general mesh partitioning the interface between the subdomains may have an infinite length which leads to some difficulties to define the absorbing boundary conditions at such interfaces.

In this paper, a coupled finite-infinite element method is described, formulated and analyzed for parallel computations purposes. This method has been successfully implemented in the SYSNOISE software, for solving huge computational acoustic problems in parallel on high performance computers or on networks of PC's. Some numerical investigations in unbounded domains, using the SYSNOISE software, are presented to demonstrate the efficiency and robustness of this method.

The scope of this paper is as follows. Section 2 describes the general scattering problem analyzed in the following. Then in Secs. 3.1 and 3.2 the finite element methods and the infinite element methods are reminded in an homogeneous formulation. Then in Sec. 3.3 the coupling between infinite and finite elements is presented. Section 4.1 presents the substructuring method followed in Sec. 4.2 by the nonoverlapping Schwarz method with zeroth order absorbing boundary conditions. Some novel discussions on the coupling between infinite and finite elements in a parallel computing context are investigated in Sec. 4.3. In Sec. 5, new numerical experiments are presented on large computational acoustics problems which demonstrate the performance and robustness of the nonoverlapping Schwarz algorithm equipped with zeroth order absorbing boundary conditions. This analysis investigates the dependency of the method upon different parameters for general mesh partitioning. Both two dimensional and three dimensional analysis are performed on academic and industrial test cases. The conclusions of our study are presented in Sec. 6.

2. Mathematical Formulation

A model radiation problem is considered in an unbounded domain. The main motivation for this analysis is to determine the frequency response functions arising from the vibrations of a structure. These vibrations can be caused by various phenomena, like a fluid flow or a wave diffraction. In the following the radiation of an object delimited by a boundary Γ_N

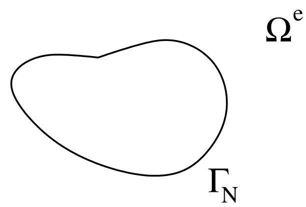

Fig. 1. Acoustic scattering problem.

immersed in an unbounded domain Ω^e, as shown in the Fig. 1 is considered. This problem can be expressed as:

$$\begin{aligned} -\triangle u - k^2 u = 0 &\qquad \text{in } \Omega^e \\ \frac{\partial u}{\partial n} = g &\qquad \text{on } \Gamma_N \\ \left|\frac{\partial u}{\partial r} - iku\right| = O(1/r^2) &\qquad \text{when } r \to +\infty \end{aligned} \tag{1}$$

where $g \in \mathbb{L}^2(\Gamma_N)$ is the prescribed Neumann boundary conditions and $k \in \mathbb{R}^+$ the wave number. The normal unitary vector along the boundary Γ_N is denoted by n, and r represents the radius in the spherical coordinates. Equation (1) is the Sommerfeld condition which ensures the propagation of the acoustic waves to infinity.

For the sake of simplicity the following equations are derived for the particular case where Γ_N is the unitary sphere, but the general case does not lead to special difficulties as will be demonstrated in the numerical experiments.

3. Infinite and Finite Element Methods

3.1. *Finite element method*

In summary, the finite element method consists of meshing the volume of a domain, for example with hexahedra, and to discretize the solution in this volume with shape basis functions, for example with $\mathbb{Q}_1$ shape functions.[15,16]

3.1.1. *Problem definition*

In the case of exterior acoustics problems, the domain of interest is unbounded and therefore cannot be meshed. The first step of the finite element method consists of defining a truncation of the unbounded domain Ω^e called Ω^e_γ as:

$$\Omega^e_\gamma = \Omega^e \cap \{x \in \mathbb{R}^3; |x| < \gamma\}$$

where the artificial boundary S_γ (here, the sphere of radius $\gamma > 1$) has been introduced. The domain Ω^e_γ is now bounded and can thus be meshed. An absorbing boundary condition is defined on the boundary S_γ. The optimal distance between the object and the artificial boundary S_γ will be dependant upon the quality of the absorbing boundary condition. The main motivation is to avoid the numerical reflections of the wave on this boundary.[7,17,6,9] The difficulty is that increasing the distance between this artificial boundary and the object increases the number of elements of the mesh.

In the following a first order approximation of the Sommerfeld boundary condition is applied on the boundary S_γ. Our initial expression can now be reformulated using the Sommerfeld boundary condition on the boundary S_γ:

$$\begin{aligned} -\triangle u - k^2 u &= 0 \qquad \text{in } \Omega_\gamma^e \\ \frac{\partial u}{\partial n} &= g \qquad \text{on } \Gamma_N \\ \frac{\partial u}{\partial r} - iku &= 0 \qquad \text{on } S_\gamma \end{aligned}$$

where $g \in \mathbb{L}^2(\Gamma_N)$ is the prescribed Neumann boundary conditions.

3.1.2. *Variational formulation*

In the variational formulation, the Helmholtz equation is first multiplied by the complex conjugate of the test function v (noted $\overline{v}$). The integration in the domain Ω_γ^e is then performed, and the Green formula is applied. The solution u belongs to the space:

$$H^1(\Omega_\gamma^e) = \{u : \|u\|_1 < \infty\}$$

with $\|u\|_1$ the norm associated to the scalar product

$$(u, v)_1 = \int_{\Omega_\gamma^e} \nabla u \nabla \overline{v}\; dV + \int_{\Omega_\gamma^e} u \overline{v}\; dV$$

where dV denotes the volume integration. After substitution of the Neumann boundary condition on Γ_N and of the Robin boundary condition on S_γ, the following variational formulation is obtained: Find $u \in H^1(\Omega_\gamma^e)$ such as

$$\int_{\Omega_\gamma^e} \nabla u \nabla \overline{v}\; dV - k^2 \int_{\Omega_\gamma^e} u \overline{v}\; dV - ik \int_{S_\gamma} u \overline{v}\; dS = \int_{\Gamma_N} g \overline{v}\; dS$$

for $\forall\, v \in H^1(\Omega_\gamma^e)$ and $g \in \mathbb{L}^2(\Gamma_N)$, where dS denotes the surface integration.

3.1.3. *Discretization*

In the cartesian coordinates system denoted by (x, y, z) in the current finite element and by (ξ, η, ζ) in the reference finite element, the approximate solution can be expressed in the form:

$$u_h(\xi, \eta, \zeta) = \sum_{j=1}^{n_e} a_j\; N_j(\xi, \eta, \zeta)$$

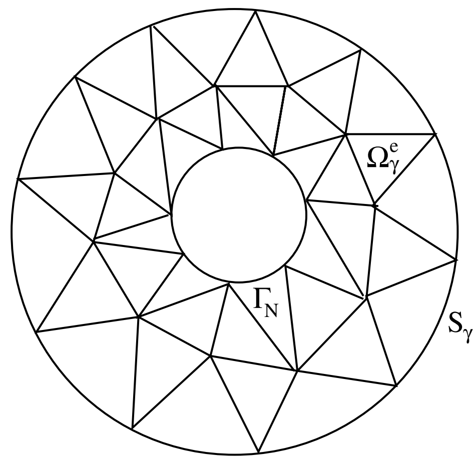

Fig. 2. Example of a finite element mesh with triangles.

with a_j the n_e unknown complex coefficients associated to the degree of freedom and N_j the basis shape functions defined on the reference finite element. For example $n_e = 8$ in the case of a discretization with $\mathbb{Q}_1$ shape functions defined on hexahedra elements. Figure 2 illustrates a finite element mesh example. After discretization of the variational formulation, the following linear system is obtained:

$$Zu_h = f$$

where f is the right hand side, and Z the impedance matrix. In the following, the subscript fem denotes a discretization with finite elements. If the degrees of freedom located inside the volume Ω_γ^e and the degrees of freedom located on the boundary S_γ are respectively denoted by subscripts i and p, the linear block matrix is obtained:

$$\begin{pmatrix} Z_{ii}^{(\mathrm{fem})} & Z_{ip}^{(\mathrm{fem})} \\ Z_{pi}^{(\mathrm{fem})} & Z_{pp}^{(\mathrm{fem})} - ikM_{pp}^R \end{pmatrix} \begin{pmatrix} x_i^{(\mathrm{fem})} \\ x_p^{(\mathrm{fem})} \end{pmatrix} = \begin{pmatrix} b_i^{(\mathrm{fem})} \\ b_p^{(\mathrm{fem})} \end{pmatrix}$$

where $Z^{(\mathrm{fem})}$ is the impedance matrix equal to $(K^{(\mathrm{fem})} - k^2 M^{(\mathrm{fem})})$ with $K^{(\mathrm{fem})}$ the volume stiffness matrix and $M^{(\mathrm{fem})}$ the volume mass matrix. The surface matrix M^R arises from the Robin boundary condition defined on S_γ. The fact that all these matrices are sparse is important to remember.

3.2. *Infinite element method*

In summary, the infinite element method consists of meshing the surface of a convex object with finite elements and to extrude this mesh to infinite. The shape basis functions includes some classical finite elements shape functions and some shape functions issue from the series expansion of the Green function. The method presented in the next section is the one first introduced in Ref. 1 and then reformulated and analyzed in Refs. 10 and 3.

3.2.1. *Variational formulation*

The first step consists of defining a truncation of the unbounded domain Ω^e called Ω^e_γ following a similar approach to that introduced in Sec. 3.1. For the particular case where the unbounded domain is the exterior of the unitary sphere, an annulus is obtained:

$$\Omega^e_\gamma = \{x \in \mathbb{R}^3; 1 < |x| < \gamma\}.$$

After the multiplication of the Helmholtz equation by the complex conjugate of the test function v, the application of the Green formula, and applying the Neumann boundary condition on Γ_N, we obtain:

$$\int_{\Omega^e_\gamma} \nabla u \nabla \overline{v}\, dV - k^2 \int_{\Omega^e_\gamma} u\overline{v}\, dV - \int_{S_\gamma} \frac{\partial u}{\partial r}\, \overline{v}\, dS = \int_{\Gamma_N} g\overline{v}\, dS.$$

The Sommerfeld condition Eq. (1) can be expressed as:

$$\frac{\partial u}{\partial r} = iku + \phi$$

where $\phi = O(1/r^2)$ is an unknown function. After substitution in the variational formulation (because $\partial u/\partial n = \partial u/\partial r$), the equation can be rewritten as:

$$\int_{\Omega^e_\gamma} \nabla u \nabla \overline{v}\, dV - k^2 \int_{\Omega^e_\gamma} u\overline{v}\, dV - ik \int_{S_\gamma} u\overline{v}\, dS = \int_{\Gamma_N} g\overline{v}\, dS + \int_{S_\gamma} \phi\overline{v}\, dS.$$

The second steps consist of taking the limit of the previous expression when γ tend to infinity. The Atkinson–Wilcox results[11] shows that the leading term of the solution u is of the form e^{ikr}/r. As a consequence, u and ∇u can no longer be integrated to infinity over $\mathbb{L}^2$. The idea consists of using special shape functions of the form $O(1/r^3)$. This helps to consider the previous integral as Lebesgue integral. With this choice, the integral on S_γ with ϕ vanishes when γ tends to infinity. The problem is that the integral on S_γ with u vanishes too. In other words, this particular choice of the tests functions does not allow to keep the Sommerfeld condition in the variational formulation. An idea proposed in Ref. 18 consists of introducing the Sommerfeld condition directly in the definition of the space. The solution u belongs to the Sobolev weighted space:

$$H^{1,+}_w(\Omega^e) = \{u : \|u\|^+_{1,w} < \infty\}$$

with $\|u\|^+_{1,w}$ the norm associated to the scalar product

$$(u,v)^+_{1,w} = \int_{\Omega^e} w \nabla u \nabla \overline{v}\, dV + \int_{\Omega^e} w u\overline{v}\, dV + \int_{\Omega^e} \left(\frac{\partial u}{\partial r} - iku\right) \overline{\left(\frac{\partial v}{\partial r} - ikv\right)}\, dV.$$

Two common weights are of interest, $w = 1/r^2$ and the dual weight $w^* = r^2$. With these notations, the variational formulation can be written: Find $u \in H^{1,+}_w(\Omega^e)$ such as

$$\int_{\Omega^e} \nabla u \nabla \overline{v}\, dV - k^2 \int_{\Omega^e} u\overline{v}\, dV = \int_{\Gamma_N} g\overline{v}\, dS$$

for $\forall\, v \in H^{1,+}_{w^*}(\Omega^e)$ and $g \in \mathbb{L}^2(\Gamma_N)$.

3.2.2. *Discretization*

A complete overview of the infinite element methods can be obtained in Refs. 12 and 11. The exact solution in the spherical coordinates system (r, θ, φ) of the current infinite element can be expended in the form (Atkinson–Wilkox):

$$u(r, \theta, \varphi) = e^{-ikr} \sum_{\kappa=1}^{\infty} \frac{G_\kappa(\theta, \varphi, k)}{r^\kappa}. \tag{3}$$

This series converges for $r > \gamma$. Considering only the first m terms of this series, and expressing these terms in the coordinates systems (ξ, η, r) of the reference infinite element leads to the approximate solution:

$$u_h(\xi, \eta, r) = e^{-ikr} \sum_{\mu=1}^{m} \frac{\widetilde{G}_\mu(\xi, \eta, k)}{r^\mu}$$

where the functions $\widetilde{G}_\mu(\xi, \eta, k)$ are defined by:

$$\widetilde{G}_\mu(\xi, \eta, k) = \sum_{\nu=1}^{n} Q_{\nu,\mu}(k)\ N_\nu(\xi, \eta)$$

with n an integer defined below. After substitution, the following expression is obtained:

$$u_h(\xi, \eta, r) = \sum_{j=1}^{n_e} a_j\ N_j(\xi, \eta, r) \quad \text{with}\, N_j(\xi, \eta, r) = N_\nu(\xi, \eta)\ N_\mu(r)$$

for $\nu = 1, \dots, n$, $\mu = 1, \dots, m$, $n_e = n \times m$, and with a_j the n_e unknowns complex coefficients associated to the degree of freedom. The shapes functions N_j are defined on the reference infinite element: N_ν denotes the angular functions with a total number of n and N_μ the radial functions with a total number of m. The integer m is called the order of the infinite element. The highest this order, the smallest the error between the approximate solution and the exact solution. Figure 3 illustrates an infinite element mesh example. The linear system issue from the discretization is the following:

$$Zu_h = f$$

where f is the right hand side, and Z the impedance matrix. In the following, the subscript ifem denotes a discretization with infinite elements. If the degrees of freedom located outside the object, i.e. in the domain Ω^e, and the degrees of freedom located on the boundary of the object Γ_N are respectively denoted by subscripts i and p, the linear block matrix is

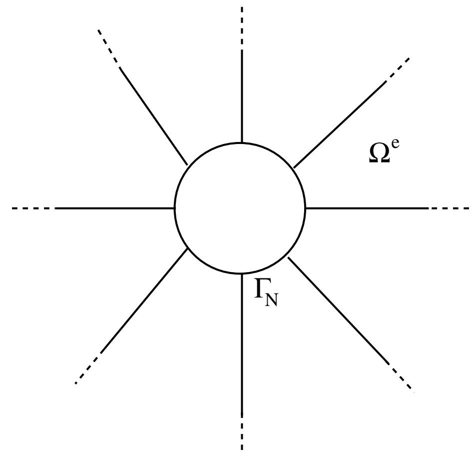

Fig. 3. Example of an infinite element mesh.

obtained:

$$\begin{pmatrix} Z_{ii}^{(\text{ifem})} & Z_{ip}^{(\text{ifem})} \\ Z_{pi}^{(\text{ifem})} & Z_{pp}^{(\text{ifem})} \end{pmatrix} \begin{pmatrix} x_i^{(\text{ifem})} \\ x_p^{(\text{ifem})} \end{pmatrix} = \begin{pmatrix} b_i^{(\text{ifem})} \\ b_p^{(\text{ifem})} \end{pmatrix}$$

where $Z^{(\text{ifem})}$ is the impedance matrix equal to $(K^{(\text{ifem})} - k^2 M^{(\text{ifem})})$ with $K^{(\text{ifem})}$ the volume stiffness matrix and $M^{(\text{ifem})}$ the volume mass matrix. It is important to point out that all these matrices are sparse matrices.

3.3. *Coupled finite-infinite element method*

The coupled finite-infinite element method consists of surrounding the object with a convex envelope. The volume between the object and the convex envelope is meshed with finite elements and infinite elements are defined on the surface of the convex envelope, as shown in Fig. 4. This approach is mandatory if ones want to use infinite elements for nonconvex objects, like a submarine for example. Indeed Eq. (3) is not valid anymore if the surface of the object is nonconvex. The solution is then discretized with finite elements basis shape functions inside the volume between the object and the envelope and with infinite elements basis shape functions outside the envelope. The linear system can be expressed as:

$$Zu_h = f$$

where f is the right hand side, and Z the impedance matrix. In the following, the subscript fem and ifem denotes a discretization with finite elements or with infinite elements respectively. If the degrees of freedom located in the domain between the object and the convex envelope, then the degrees of freedom located outside the convex envelope, and finally the degrees of freedom located on the convex envelope are respectively numbered, the linear

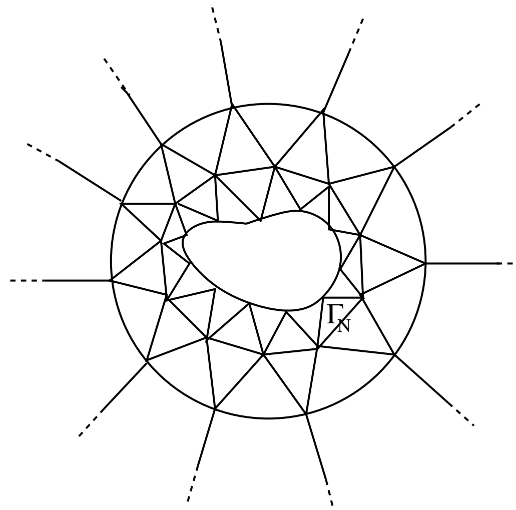

Fig. 4. Coupled finite-infinite element mesh.

block matrix is obtained:

$$\begin{pmatrix} Z_{ii}^{(\text{fem})} & 0 & Z_{ip}^{(\text{fem})} \\ 0 & Z_{ii}^{(\text{ifem})} & Z_{ip}^{(\text{ifem})} \\ Z_{pi}^{(\text{fem})} & Z_{pi}^{(\text{ifem})} & Z_{pp}^{(\text{fem})} + Z_{pp}^{(\text{ifem})} \end{pmatrix} \begin{pmatrix} x_i^{(\text{fem})} \\ x_i^{(\text{ifem})} \\ x_p \end{pmatrix} = \begin{pmatrix} b_i^{(\text{fem})} \\ b_i^{(\text{ifem})} \\ b_p^{(\text{fem})} + b_p^{(\text{ifem})} \end{pmatrix}$$

where the above mentioned matrices have been defined in the previous section. The previous numbering of the degrees of freedom is very similar to the sub-structuring methodology, as presented in the following section.

4. Parallel Computing

4.1. *Sub-structuring methods*

Let us now consider in detail a number of algorithms to solve the linear system $Zu_h = f$ efficiently on parallel computers. The following discretization scheme is presented for a decomposition of a general domain Ω into two subdomains $\Omega^{(1)}$ and $\Omega^{(2)}$ with an interface Γ as shown in Fig. 5. The domain Ω is meshed with finite elements only. The degrees of freedom located inside subdomain $\Omega^{(s)}$, $s = 1, 2$ and on the interface Γ are denoted by subscripts i and p. With this notation the contribution of subdomain $\Omega^{(s)}$, $s = 1, 2$ to the impedance matrix and to the right-hand side can be written as in Refs. 19 and 20:

$$Z^{(s)} = \begin{pmatrix} Z_{ii}^{(s)} & Z_{ip}^{(s)} \\ Z_{pi}^{(s)} & Z_{pp}^{(s)} \end{pmatrix}, \quad b^{(s)} = \begin{pmatrix} b_i^{(s)} \\ b_p^{(s)} \end{pmatrix}, \quad s = 1, 2.$$

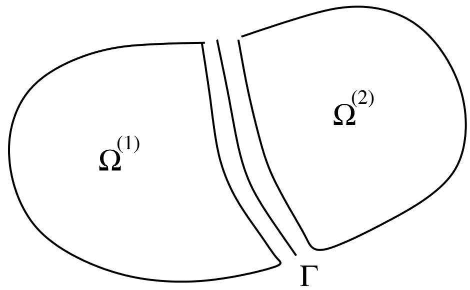

Fig. 5. Nonoverlapping domain splitting.

The global problem is a block system obtained by assembling the local contributions from each subdomain:

$$\begin{pmatrix} Z_{ii}^{(1)} & 0 & Z_{ip}^{(1)} \\ 0 & Z_{ii}^{(2)} & Z_{ip}^{(2)} \\ Z_{pi}^{(1)} & Z_{pi}^{(2)} & Z_{pp} \end{pmatrix} \begin{pmatrix} x_i^{(1)} \\ x_i^{(2)} \\ x_p \end{pmatrix} = \begin{pmatrix} b_i^{(1)} \\ b_i^{(2)} \\ b_p \end{pmatrix}. \tag{4}$$

The matrices $Z_{pp}^{(1)}$ and $Z_{pp}^{(2)}$ represent the interaction matrices between the nodes on the interface obtained by integration on $\Omega^{(1)}$ and on $\Omega^{(2)}$. The block Z_{pp} is the sum of these two blocks. In a same way the term $b_p = b_p^{(1)} + b_p^{(2)}$ is obtained by local integration of the right hand side over each subdomain and the summation on the interface.

In order to solve this linear system with an iterative method, a matrix vector product of the matrix Z by a descent direction vector $w = (w_i^{(1)}, w_i^{(2)}, w_p)^T$ should be computed at each iteration. This matrix vector product can be performed using the previous sub-structuring expression in two successive steps:

- Computation of local matrix vector product in each subdomain:

$$\begin{pmatrix} v_i^{(1)} \\ v_p^{(1)} \end{pmatrix} = \begin{pmatrix} Z_{ii}^{(1)} & Z_{ip}^{(1)} \\ Z_{pi}^{(1)} & Z_{pp}^{(1)} \end{pmatrix} \begin{pmatrix} w_i^{(1)} \\ w_p \end{pmatrix}, \quad \begin{pmatrix} v_i^{(2)} \\ v_p^{(2)} \end{pmatrix} = \begin{pmatrix} Z_{ii}^{(2)} & Z_{pi}^{(2)} \\ Z_{pi}^{(2)} & Z_{pp}^{(2)} \end{pmatrix} \begin{pmatrix} w_i^{(2)} \\ w_p \end{pmatrix}.$$

- Assembly of the vectors on the interface:

$$v_p = v_p^{(1)} + v_p^{(2)}$$

which gives the vector $v = (v_i^{(1)}, v_i^{(2)}, v_p)^T$. In the case of a general multi-domain mesh splitting, adding the contributions of the local dot products will introduce a weighting factor per node in the dot product equal to the number of subdomains the node belongs to. A weighting vector on the interface must be introduced in order to avoid having to consider multiple contribution of the vector component at such cross points.

4.2. *Domain decomposition methods*

The previous sub-structuring method requires at each iteration a local matrix vector product, which is computed in parallel in each subdomain, and assembly of the vectors on the interface between the subdomain. This method is very easy to implement,[13] but the convergence may be difficult to achieve in the case of large acoustic problems without preconditioning techniques. In order to improve the convergence speed of the iterative algorithm, some preconditioning techniques based on domain decomposition methods are an efficient alternative. The nonoverlapping Schwarz method for example involves an iterative method (performed on the degrees of freedom located on the interface) and a local matrix factorization (on the degrees of freedom located inside each subdomain). At each iteration a local forward backward substitution is involved in each subdomain, and assembly on the interface. This algorithm is based on the following theorem.

Theorem 4.1. *Under a splitting of the form* $Z_{pp} = Z_{pp}^{(1)} + Z_{pp}^{(2)}$ *and* $b_p = b_p^{(1)} + b_p^{(2)}$, *for all matrices* $A^{(1)}$, $A^{(2)}$ *there is one and only one associated value* $\lambda^{(1)}$, $\lambda^{(2)}$ *such as the following coupled problems*:

$$\begin{pmatrix} Z_{ii}^{(1)} & Z_{ip}^{(1)} \\ Z_{pi}^{(1)} & Z_{pp}^{(1)} + A^{(1)} \end{pmatrix} \begin{pmatrix} x_i^{(1)} \\ x_p^{(1)} \end{pmatrix} = \begin{pmatrix} b_i^{(1)} \\ b_p^{(1)} + \lambda^{(1)} \end{pmatrix} \tag{5}$$

$$\begin{pmatrix} Z_{ii}^{(2)} & Z_{ip}^{(2)} \\ Z_{pi}^{(2)} & Z_{pp}^{(2)} + A^{(2)} \end{pmatrix} \begin{pmatrix} x_i^{(2)} \\ x_p^{(2)} \end{pmatrix} = \begin{pmatrix} b_i^{(2)} \\ b_p^{(2)} + \lambda^{(2)} \end{pmatrix} \tag{6}$$

$$x_p^{(1)} - x_p^{(2)} = 0 \tag{7}$$

$$\lambda^{(1)} + \lambda^{(2)} - A^{(1)} x_p^{(1)} - A^{(2)} x_p^{(2)} = 0 \tag{8}$$

are equivalent to the problem (4).

Proof. The admissibility condition (7) derives from the relation $x_p^{(1)} = x_p^{(2)} = x_p$.

If $x_p^{(1)} = x_p^{(2)} = x_p$, the first rows of local systems (5) and (6) are the same as the two first rows of the global system (4), and adding the last rows of the local systems (5) and (6) gives:

$$Z_{pi}^{(1)} x_i^{(1)} + Z_{pi}^{(2)} x_i^{(2)} + Z_{pp}\, x_p - b_p = \lambda^{(1)} + \lambda^{(2)} - A^{(1)} x_p^{(1)} - A^{(2)} x_p^{(2)}.$$

So, the last equation of global system (4) is satisfied only if:

$$\lambda^{(1)} + \lambda^{(2)} - A^{(1)} x_p^{(1)} - A^{(2)} x_p^{(2)} = 0.$$

Conversely, if $x_p^{(1)}$, $x_p^{(2)}$ and x_p are derived from the global system (4), then the local systems (5) and (6) define $\lambda^{(1)}$ and $\lambda^{(2)}$ in a unique way. □

The complete nonoverlapping Schwarz algorithm consists of searching iteratively for the value of $(\lambda^{(1)}, \lambda^{(2)})^T$ such as the value of $(x_p^{(1)}, x_p^{(2)})^T$ satisfy Eqs. (7) and (8). The only restriction imposed on the matrices $A^{(1)}$ and $A^{(2)}$ in the previous theorem is that for a given right hand side the local sub-problems defined in Eqs. (5) and (6) have an unique solution. The elimination of $x_i^{(1)}$ and $x_i^{(2)}$ in favor of $x_p^{(1)}$ and $x_p^{(2)}$ in the previous equations leads to the following linear system:

$$\begin{pmatrix} I & I - (A^{(1)} + A^{(2)})[S^{(2)} + A^{(2)}]^{-1} \\ I - (A^{(1)} + A^{(2)})[S^{(1)} + A^{(1)}]^{-1} & I \end{pmatrix} \begin{pmatrix} \lambda^{(1)} \\ \lambda^{(2)} \end{pmatrix}$$
$$= \begin{pmatrix} (A^{(1)} + A^{(2)})[S^{(2)} + A^{(2)}]^{-1} c_p^{(2)} \\ (A^{(1)} + A^{(2)})[S^{(1)} + A^{(1)}]^{-1} c_p^{(1)} \end{pmatrix} \tag{9}$$

where $S^{(q)} = Z_{pp}^{(q)} - Z_{pi}^{(q)} [Z_{ii}^{(q)}]^{-1} Z_{ip}^{(q)}$ is the condensed matrix and $c_p^{(q)} = b_p^{(q)} - Z_{pi}^{(q)} [Z_{ii}^{(q)}]^{-1} b_i^{(q)}$ is the condensed right hand side, for $q = 1, 2$. This linear system is solved with an iterative method, and each iteration involves a solution of an Helmholtz sub-problem in each subdomain.

The choice of the matrices $A^{(1)}$ and $A^{(2)}$ has a strong influence on the convergence speed of the nonoverlapping Schwarz algorithm. Different choice of these matrices has been investigated in Refs. 21–23. In the following the matrices $A^{(1)}$ and $A^{(2)}$ are obtained from a Taylor zeroth order approximation of the Steklov–Poincaré operator and from an optimized zeroth order approximation of the Steklov–Poincaré operator for internal acoustics problems discretized with finite elements, as introduced in Ref. 23. These matrices are equal to

$$A^{(1)} := \alpha\ M_\Gamma, \quad A^{(2)} := \alpha\ M_\Gamma$$

where α is equal to ik for a Taylor zeroth order approximation and obtained from the solution of a minimization problem for an optimized zeroth order approximation.[24] The matrix M_Γ is a surface mass matrix defined on the interface between the subdomains.

4.3. *Coupling finite and infinite element*

When a general mesh partitioning of the global domain is performed, the interface joins some (finite or infinite) elements sharing a common edge on the interface and belonging to different subdomains. Three possibilities may appear: two finite elements sharing an edge on the interface, or one finite element and one infinite element sharing an edge on the interface, or two infinite elements sharing an edge on the interface. In this last case the length of the interface is infinite.

If some Lagrange finite elements are considered, for example $\mathbb{P}_1$-finite elements, the degrees of freedom of an element corresponds to the nodes of the triangle. Defining the Lagrange multipliers at the nodes of the finite element helps to apply the sub-structuring methodology described Sec. 4.2. Figure 6 shows the definition of the degrees of freedom and of the Lagrange multipliers for two finite elements sharing one edge on the interface.

In the second case, the Lagrange multipliers should be defined at the element nodes as shown in Fig. 7. Indeed in this case, the restriction on the edge of the angular basis functions

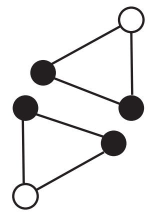

Fig. 6. Definition of the degree of freedom (white and black bullets) of the elements and of the Lagrange multipliers (black bullets) between two finite elements.

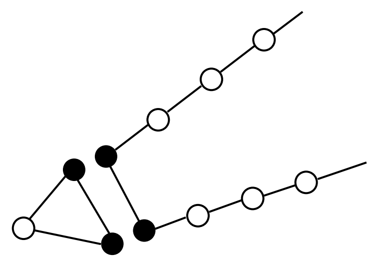

Fig. 7. Definition of the degree of freedom (white and black bullets) of the elements and of the Lagrange multipliers (black bullets) between an infinite element and a finite element.

of the infinite element is similar to the restriction of the $\mathbb{P}_1$-finite element basis functions. As a consequence, there is no difference between this case and the previous one.

In the third case, the Lagrange multipliers should be defined at the element nodes and at the Gauss points of the infinite elements as shown in Fig. 7. These Gauss points correspond to the degree of freedom of the infinite element and are used to compute the integrals of Sec. 3.2. Increasing the order of the infinite element implies increasing the number of Gauss points and so far the number of Lagrange multipliers. As a consequence the size of the linear system defined Eq. (9) becomes much bigger. A second consequence is that increasing the order of the infinite element tends to deteriorate the conditioning number of the assembly matrix.

In summary, the Lagrange multipliers are simply defined on the degrees of freedom. This can be the nodes of the elements (for finite elements) or the Gauss points (for the infinite elements). If zeroth order absorbing boundary conditions are considered in the nonoverlapping Schwarz algorithm, a surface mass matrix should be computed on the interface between the subdomain. This matrix is of the form:

$$M_\Gamma = \int_\Gamma uv \; dS.$$

In the case of an interface between two finite elements, the coefficients of the matrix M_Γ are computed as:

$$[M_\Gamma]_{lm} = \int_{\Omega^{(1)} \cap \Omega^{(2)}} N_l N_m \; dS$$

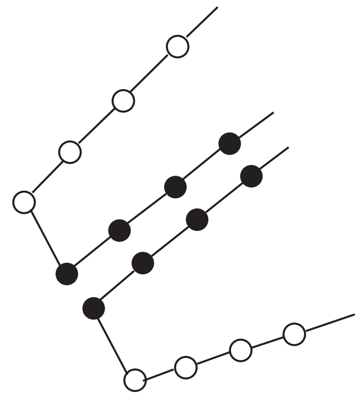

Fig. 8. Definition of the degree of freedom (white and black bullets) of the elements and of the Lagrange multiplier (black bullets) between two infinite elements.

where N_l and N_m are the finite element shape functions associated with node l and node m on the common edge on the interface between subdomains $\Omega^{(1)}$ and $\Omega^{(2)}$. In the case of an interface between one finite element and one infinite element, the finite element shape functions on the common edge is similar to the angular infinite element shape function i.e. the functions N_ν. When two infinite elements share a common edge, the integral along this infinite edge only involves the radial shape functions i.e. the functions N_μ, and the integral is computed using the Gauss points along the infinite edge.

5. Numerical Experiments

5.1. *Radiation of an infinite cylinder*

In this section the convergence properties of the parallel iterative GMRES preconditioned by the diagonal versus the nonoverlapping Schwarz method are analyzed. The behavior of these methods upon different parameters is investigated.

The test case consist of a multi-pole radiation of an infinite cylinder of radius a. Due to the symmetry of the geometry, only one half cross section is considered for the analysis. The radiation of the cylinder is generated by the vibration of the surface. These vibration are modeled by a normal acceleration of the particles along the surface. The normal velocity distribution is defined by the relation $V_n(\theta) = V \cos(p\theta)$ where θ denotes the angle in cylindric coordinates and where $p = 0, 1, 2 \ldots$ for a multi-pole of order $0, 1, 2 \ldots$. An artificial boundary is defined on an infinite cylinder of radius $1.5a$. The volume between the cylinder and the artificial boundary is meshed with quadrilateral finite elements. Infinite elements are defined on the surface of the artificial boundary. Because of the order p of the multi-pole, the order of the infinite elements should be at least equal to $m = p + 1$, see Ref. 3. The six elements per wavelength criteria is ensured over all the mesh presented in Fig. 9. The domain is then split in subdomains with a geometric based algorithm, in such a way that each subdomain has at most two neighboring subdomains as shown in Fig. 10. The mesh partitioning software ensures a load balancing distribution of the degree of freedom

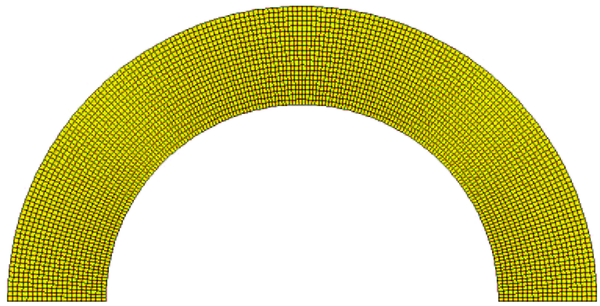

Fig. 9. Radiation of an infinite cylinder: Finite element mesh.

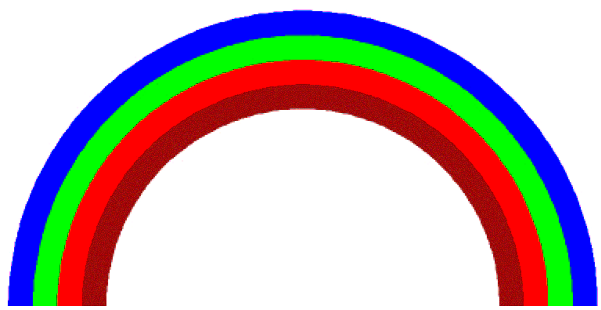

Fig. 10. Radiation of an infinite cylinder: Mesh partitioning.

in each subdomain. This decomposition has first the advantage of reducing the numerical error by ensuring that the interfaces between the subdomains are parallel to the cylinder. Secondly, this decomposition presents the advantage of collecting all the infinite elements in the same subdomain. The acoustic solution of a multi-pole of order four is presented in Fig. 11. The parameters indicated are the radius of the infinite cylinder a, the mesh size h, the wave number k, the order of the infinite element m, the order of the multi-pole p, and the number of subdomains N_s, respectively.

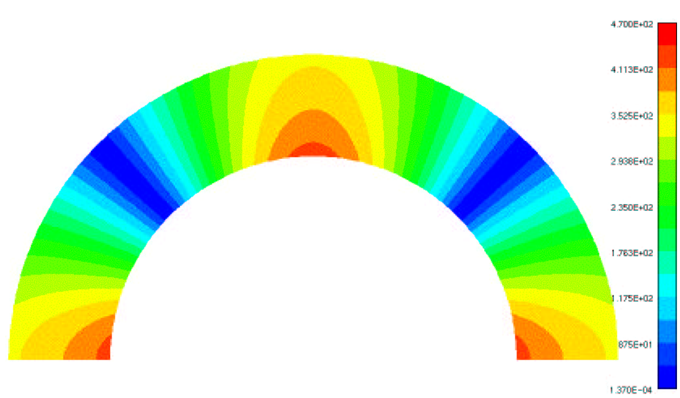

Fig. 11. Radiation of an infinite cylinder: Acoustic pressure.

The parallel iterative GMRES preconditioned by the diagonal and the nonoverlapping Schwarz method have been implemented in the SYSNOISE software for trial purpose. The condensed interface problem of the nonoverlapping Schwarz algorithm is solved with the GMRES algorithm, and local Crout factorizations are performed in each subdomain. The CPU time indicated for the nonoverlapping Schwarz algorithm is the total CPU time, including the factorization of the matrix. The convergence is analyzed with the following stopping criteria

$$\|Zu_h - f\|_{\mathbb{L}_2} \leq 10^{-8} \; \|f\|_{\mathbb{L}_2}$$

where $\|f\|_{\mathbb{L}_2}$ denotes the module of the complex number $\overline{f}f$. The numerical simulation are performed on a SGI Origin 200 with four processors.

As expected from the theory, the convergence speed of the nonoverlapping Schwarz algorithm is weakly dependent upon the mesh size, see Table 1. On the contrary the parallel GMRES preconditioned by the diagonal presents a strong dependance upon this parameter. As already reported for internal acoustic problems,[24] the nonoverlapping Schwarz algorithm performs up to 35% better with an optimized zeroth order (OO0) absorbing boundary conditions than with a Taylor zeroth order (TO0) absorbing boundary conditions.

The results presented in Table 2 illustrate the dependence upon the wave number. Once again, the good convergence properties of the nonoverlapping Schwarz method with zeroth order absorbing boundary conditions can be noticed.

Since the number of iterations of the preconditioned GMRES does not depend upon the number of subdomains resulting from the mesh partitioning, the results reported in Table 3 may appear disappointing. However, increasing the number of subdomains in the GMRES method increases the number of data exchange between the processors, and each iteration requires more time. For this reason the nonoverlapping Schwarz algorithm is still very competitive.

Finally the results reported in Table 4 illustrate the dependence of the methods upon the order of the infinite element. Since all the infinite elements are collected in the same subdomains, and because the nonoverlapping Schwarz algorithm involves a direct solution inside each subdomains, the dependence is very weak. This dependence even disappears

Table 1. Number of iterations versus the mesh size parameter for the radiation problem. The multi-pole order is equal to $p = 2$, the wave number equal to $ka = 20$, and the order of the infinite element equal to $m = 3$. A total number of $N_s = 4$ subdomains have been used for the simulation.

	GMRES with Diag. Prec.		Schwarz with TO0		Schwarz with OO0	
h	# Iterations	CPU	# Iterations	CPU	# Iterations	CPU
1/24	723	$\gg$ 10 sec	239	2 sec	159	1 sec
1/32	972	$\gg$ 10 sec	229	4 sec	164	2 sec
1/40	1248	$\gg$ 10 sec	262	8 sec	169	4 sec

Table 2. Number of iterations versus the wave number parameter for the radiation problem. The multi-pole order is equal to $p = 2$, the mesh size parameter equal to $h = 1/40$, and the order of the infinite element equal to $m = 3$. A total number of $N_s = 4$ subdomains have been used for the simulation.

	GMRES with Diag. Prec.		Schwarz with TO0		Schwarz with OO0	
ka	# Iterations	CPU	# Iterations	CPU	# Iterations	CPU
10	980	$\gg$ 40 sec	152	7 sec	101	4 sec
20	1248	$\gg$ 40 sec	262	8 sec	169	4 sec
30	1523	$\gg$ 40 sec	412	9 sec	245	6 sec
40	1781	$\gg$ 40 sec	463	9 sec	301	6 sec

Table 3. Number of iterations versus the number of subdomains for the radiation problem. The multi-pole order is equal to $p = 2$, the mesh size parameter equal to $h = 1/40$, the wave number equal to $ka = 40$, and the infinite element order parameter equal to $m = 3$.

	GMRES with Diag. Prec.		Schwarz with TO0		Schwarz with OO0	
N_s	# Iterations	CPU	# Iterations	CPU	# Iterations	CPU
2	1781	$\gg$ 40 sec	150	5 sec	121	4 sec
3	1781	$\gg$ 40 sec	294	6 sec	186	4 sec
4	1781	$\gg$ 40 sec	463	9 sec	301	6 sec
5	1781	$\gg$ 40 sec	650	12 sec	337	6 sec
6	1781	$\gg$ 40 sec	691	12 sec	383	7 sec

Table 4. Number of iterations versus the infinite element order for the radiation problem. The multi-pole order is equal to $p = 2$, the mesh size parameter equal to $h = 1/40$, the wave number equal to $ka = 40$. A total number of $N_s = 4$ subdomains have been used for the simulation.

	GMRES with Diag. Prec.		Schwarz with TO0		Schwarz with OO0	
m	# Iterations	CPU	# Iterations	CPU	# Iterations	CPU
3	1781	$\gg$ 40 sec	463	9 sec	301	6 sec
4	1933	$\gg$ 40 sec	449	8 sec	301	6 sec
5	2087	$\gg$ 40 sec	465	9 sec	306	6 sec
6	2216	$\gg$ 40 sec	475	9 sec	307	6 sec

when the nonoverlapping Schwarz algorithm is equipped with an optimized zeroth order absorbing boundary conditions.

5.2. *Acoustic scattering*

In this section a three dimensional acoustic scattering problem where the obstacle has the shape of a submarine is analyzed. The length of the submarine is equal to 76 meters, the height equal to 9.25 meters and the diameter equal to 7.5 meters. The characteristic of the ocean are a density equal to $1000\,\mathrm{kg/m^3}$ and a sound speed equal to $c = 1500\,\mathrm{m/s}$. The goal of this analysis consists of evaluating the frequency response functions generated by the vibration of the structure of the submarine issue from the scattering of an incident wave. The computing steps can be expressed as the following sequence:

- An incident planar wave is defined in the ocean and strikes the submarine. A coupled fluid-structure computation is performed. The fluid is discretized with boundary elements and the structure of the submarine is discretized with shell finite element. The solution, i.e. the acoustic pressure for the fluid and the displacement for the structure, of this coupled problem are obtained for different frequencies.
- An acoustic computation is then performed. The ocean around the submarine is discretized with coupled finite-infinite elements. An ellipsoid is defined around the submarine and the volume between the submarine and the ellipsoid is meshed with finite elements. Infinite elements are defined on the surface of the ellipsoid. The criteria of six nodes per wavelength is satisfied over all the mesh. The final mesh is composed with 32 000 nodes, 162 000 tetrahedra finite elements and 11 500 infinite elements. Using the displacement of the structure of the submarine — given by the fluid-structure problem — as the boundary conditions of the acoustic problem, the acoustic pressure can be obtained for different frequencies.

The fluid-structure computation is performed with the MSC-NASTRAN software. The acoustic problem is solved with the SYSNOISE software equipped with the nonoverlapping Schwarz method.

Figure 12 shows the shape of the submarine, whilst Fig. 13 shows the finite element mesh of the volume between the submarine and the ellipsoid. Two examples of mesh partitioning are presented in Figs. 14 and 15. These two mesh partitionings generate load balancing subdomains. Figure 14 presents a geometric based mesh partitioning. In this case all the infinite elements are located in the same subdomain. The coupling between the only subdomain — with all the infinite elements — and the only neighboring subdomain — with only finite elements — becomes similar to the coupling between two subdomains — with only finite elements. Figure 15 presents a mesh partitioning performed with the METIS software.[25,26] In this case, the mesh partitioning generates subdomains which can share a common infinite interface. Figure 16 shows the acoustic pressure in decibel in the ocean around the

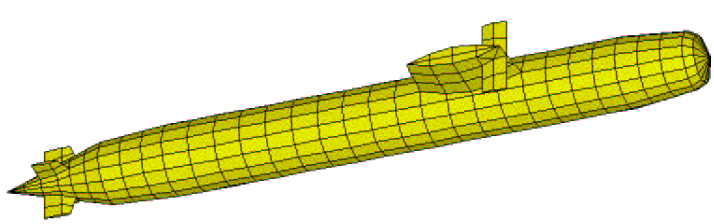

Fig. 12. Submarine acoustic problem: Geometry.

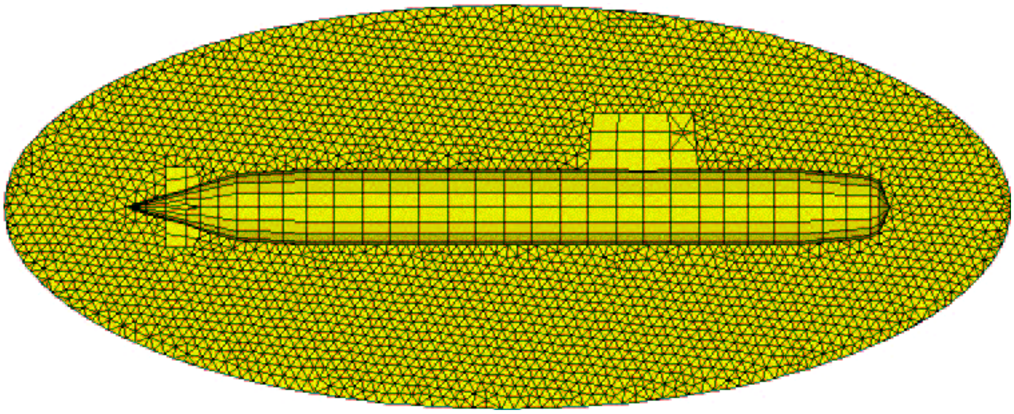

Fig. 13. Submarine acoustic problem: Finite element mesh.

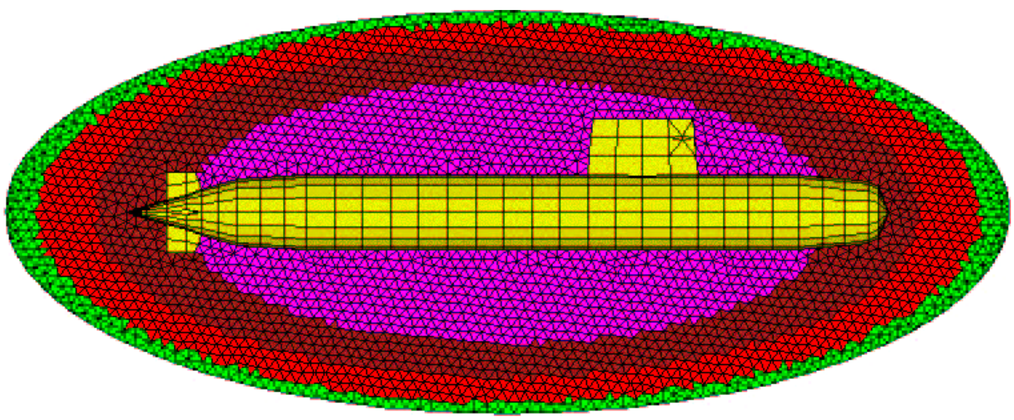

Fig. 14. Submarine acoustic problem: Geometric based mesh partitioning.

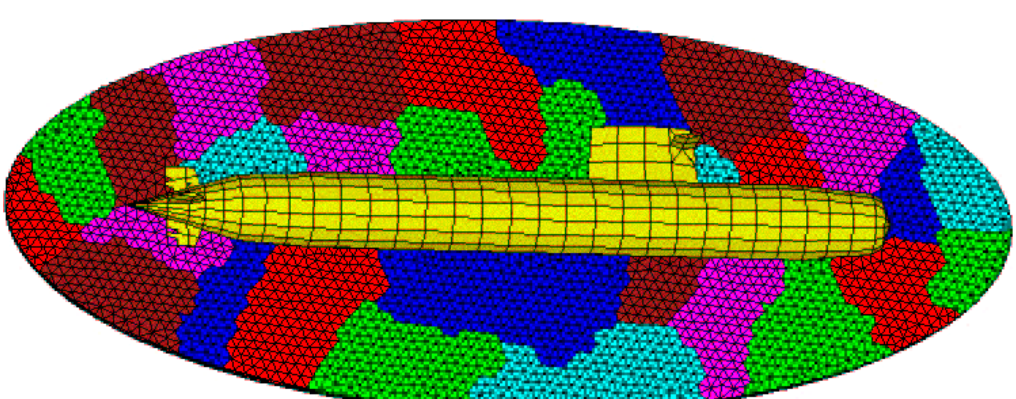

Fig. 15. Submarine acoustic problem: METIS mesh partitioning.

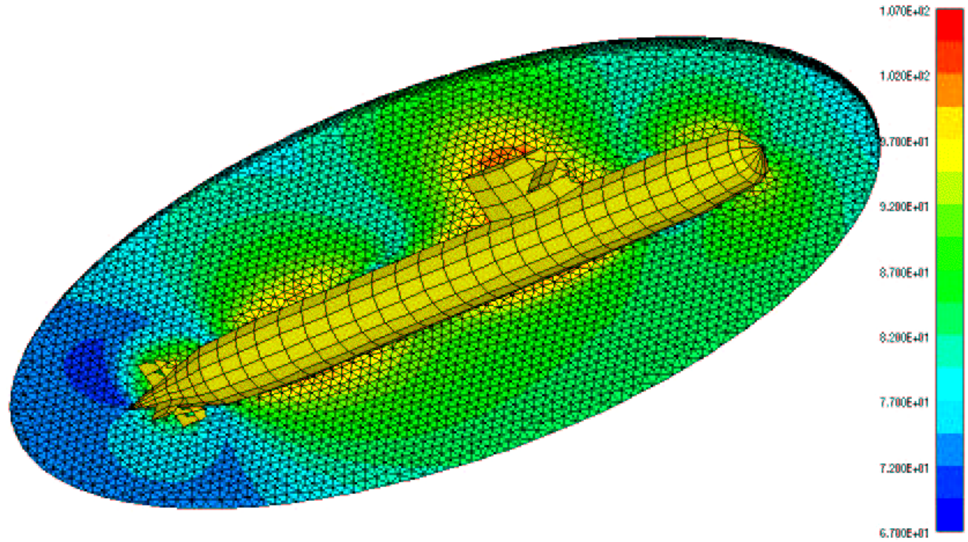

Fig. 16. Submarine acoustic problem: Acoustic pressure in decibel.

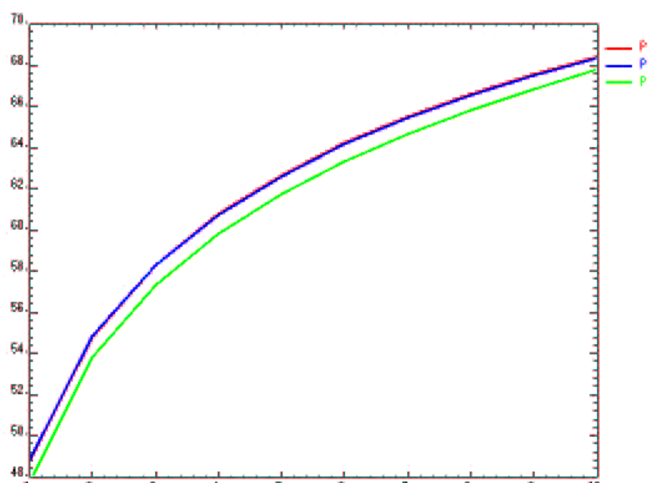

Fig. 17. Submarine acoustic problem: Comparison of frequency responses function for a solution computed with coupled finite-infinite element versus a solution computed with boundary element.

submarine for a frequency equal to 10 Hz. Figure 17 represents the accuracy of the coupled finite-infinite elements solution compared to the solution computed with boundary elements. An infinite element order equal to three is mandatory in order to ensure the same accuracy between the coupled finite-infinite element computation, and the boundary element computation. Bearing in mind that increasing the frequency requires a finer mesh and will increase the dimension of the dense matrix issued from the boundary element method. For such high frequencies, the coupled finite-infinite element, which keeps the sparsity of the matrix, is definitely a good alternative to the boundary element method.

Tables 5 and 6 present the convergence results for a frequency equal to 47 Hz and a stopping criteria equal to 10^{-8}. The first table consider a mesh partitioning based on a geometric algorithm, and the second table consider a mesh partitioning with METIS.

In Table 5, similar properties than in the previous subsection can be noticed. The GMRES algorithm is not presented here since for this simulation this algorithm would require more than 1000 iterations and more than 3600 seconds CPU time, compared to 423 seconds CPU time for the nonoverlapping Schwarz algorithm with an optimized zeroth order absorbing boundary conditions.

Table 5. Number of iterations for different number of subdomains and different infinite element order for the submarine acoustic problem. The wave number is equal to $ka = 0.2$, and the mesh partitioning is based on a geometric algorithm.

		Schwarz with TO0		Schwarz with OO0	
N_s	m	# Iterations	CPU	# Iterations	CPU
2	3	36	780 sec	24	530 sec
—	4	36	780 sec	24	530 sec
—	5	38	797 sec	24	530 sec
3	3	106	540 sec	70	420 sec
—	4	108	551 sec	71	425 sec
—	5	108	551 sec	71	425 sec
4	3	113	570 sec	73	408 sec
—	4	113	570 sec	73	408 sec
—	5	115	576 sec	75	421 sec

Table 6. Number of iterations for different number of subdomains and different infinite element order for the submarine acoustic problem. The wave number is equal to $ka = 0.2$, and the mesh partitioning is obtained with METIS.

		Schwarz with TO0	Schwarz with OO0
N_s	m	# iterations	# iterations
8	3	86	57
—	4	90	59
—	5	94	61
16	3	210	139
—	4	221	144
—	5	232	151
32	3	422	280
—	4	438	294
—	5	456	307

The results presented in Table 6 show the dependence of the nonoverlapping Schwarz algorithm upon the number of subdomains and upon the order of the infinite element for a general mesh partitioning.

6. Conclusions

In this paper, a review of the finite element method and of the infinite element method is first presented. Then the coupled finite-infinite element method is described in detail. This coupled method is interesting for solving acoustic scattering problems in unbounded domain involving nonconvex scattered objects. The description of two parallel algorithms implemented in the SYSNOISE software is then presented. The first algorithm consists of a parallel preconditioned iterative method. The second algorithm consists of a parallel nonoverlapping Schwarz method with absorbing boundary conditions defined on the interface between the subdomains. The definition of these absorbing boundary conditions in the case of a finite and/or an infinite interface is analyzed. Then the parallel preconditioned iterative method and the parallel nonoverlapping Schwarz method with zeroth order absorbing boundary are compared. A wide range of numerical experiments are studied for computational acoustics scattering problems in unbounded domains that demonstrate the performance and robustness of the nonoverlapping Schwarz method with zeroth order absorbing boundary conditions.

Acknowledgments

The authors would like to acknowledge J.-P. Coyette and K. Gerdès for the useful discussions, comments and remarks on this paper.

References

1. J. Astley, J. Macaulay and J. P. Coyette, Mapped wave envelope elements for acoustical radiation and scattering, *J. Sound and Vibration* **170**(1) (1994) 97–118.
2. D. Burnett, A 3-d acoustic infinite element based on a generalized multipole expansion, *J. Acoust. Soc. Am.* **96**(5) (1994) 2798–2816.
3. K. Gerdes, Solution of the 3D Laplace and Helmholtz equation in exterior domains of arbitrary shape using hp-finite-infinite elements, PhD thesis, University of Texas at Austin (1996).
4. G. Chen and J. Zhou, *Boundary Element Methods* (Academic Press London, 1992).
5. M. Costabel, Symmetric methods for the coupling of finite elements and boundary elements, in *Boundary Elements IV, Vol. 1, Comput. Mech.* (Brebier, Southampton, 1987), pp. 441–420.
6. B. Engquist and A. Majda, Absorbing boundary conditions for the numerical simulation of waves, *Math. Comp.* **31**(139) (1977) 629–651.
7. L. Halpern, Absorbing boundary conditions for the discretization schemes of the one dimensional wave equation, *Math. Comp.* **38** (1982) 415–429.
8. D. Givoli, High-order non-reflecting boundary conditions without high-order derivatives, *J. Comp. Phys.* **170** (2001) 849–870.
9. D. Givoli and B. Neta, High-order non-reflecting boundary conditions for dispersive waves, *Wave Motion* **37** (2003) 257–271.

10. R. J. Astley, G. J. Macaulay, J. P. Coyette and L. Cremers, Three-dimensional wave envelope elements of variable order for acoustic radiation and scattering — Part I: Formulation in the frequency domain **103** (1998) 49–63.
11. F. Ihlenburg, *Finite Element Analysis of Acoustic Scattering* (Springer, 1998).
12. K. Gerdes, A review of infinite element methods for exterior helmholtz problems, *J. Comp. Acoust.* **8**(1) (2000).
13. F. Magoulès, F.-X. Roux, J.-P. Coyette and C. Lecomte, Numerical treatment of internal acoustic problems by substructuring methods, in *International Conference on Advanced Computational Methods in Engineering* (Ghent, Belgium, September 1998).
14. F. Magoulès and J.-C. Autrique, Calcul parallèle et méthodes d'éléments finis et infinis pour des problèmes de radiation acoustique, *Calculateurs Parallèles, Réseaux et Systèmes Répartis*, **13**(1) (2001) [Hermès].
15. P. G. Ciarlet, *The Finite Element Method for Elliptic Problems* (North-Holland, Amsterdam, 1978).
16. K.-J. Bathe, *Finite Element Procedures* (Prentice Hall, New Jersey, 1996).
17. P. Joly and O. Vacus, Sur l'analyse des conditions aux limites absorbantes pour l'équation de Helmholtz. rapport de recherche 28–50, INRIA (1996).
18. R. Leis, *Initial Boundary Value Problems in Mathematical Physics* (Teubner, 1986).
19. C. Farhat and F.-X. Roux, Implicit parallel processing in structural mechanics, in *Computational Mechanics Advances*, ed. J. T. Oden, Vol. 2(1) (North-Holland, 1994), pp. 1–124.
20. B. F. Smith, P. E. Bjørstad and W. Gropp, *Domain Decomposition: Parallel Multilevel Methods for Elliptic Partial Differential Equations* (Cambridge University Press, 1996).
21. M. J. Gander, Optimized Schwarz methods for Helmholtz problems, in *12th International Conference on Domain Decomposition Methods* (2000), pp. 247–254.
22. F. Magoulès, Parallel algorithms for time-harmonic hyperbolic problems, in *Computational Mechanics Using High Performance Computing*, ed. B. H. V. Topping, Chapter 8 (Saxe-Coburg Publications, 2002), pp. 151–183.
23. M. J. Gander, F. Magoulès and F. Nataf, Optimized Schwarz methods without overlap for the Helmholtz equation, *SIAM J. Scientific Computing* **24**(1) (2002) 38–60.
24. F. Magoulès, *Méthodes numériques de décomposition de domaine pour des problèmes de propagation d'ondes*, PhD thesis, Université Pierre & Marie Curie (Jan 2000).
25. G. Karypis and V. Kumar, METIS — unstructured graph partitioning and sparse matrix ordering system — version 2.0. Technical report, University of Minnesota, Dept. Computer Science, Minneapolis MN 55455 (1995).
26. G. Karypis and V. Kumar, METIS: A software package for partitioning unstructured graphs, partitioning meshes, and computing fill-reducing orderings of sparse matrices. Available via http://www.cs.umn.edu/∼karypis, 1997.